

# Chapter 1

## Introduction

### 1.1 The Multi-Messenger Astrophysics

Our understanding of the Universe has been continuously updated with the emergence of new techniques of astronomical observations. Since the time of Galileo, we have accumulated knowledge of the astronomical object and the Universe itself based on the information carried by visible light. Multi-wavelength astronomy was established and developed during the last few decades as the advancing radio, infrared, ultra-violet, optical, X-ray, and  $\gamma$ -ray telescopes were built. In contrast to the long-standing use of the first messenger produced by the electromagnetic (EM) force, the astrophysical applications of messengers such as cosmic rays (CRs), neutrinos, and gravitational waves (GWs), were realized after the mid-20th century. Currently, we are able to combine the unique properties of two or more of these messengers to explore the physics of astrophysical phenomena from different perspectives.

#### 1.1.1 Electromagnetic (EM) Photons

Extensive multi-wavelength studies of the EM emissions from gamma-ray bursts (GRBs), tidal disruption events (TDEs), supernovae, active galactic nuclei (AGNs), and galaxies had provided valuable information to construct the theoretical models before the CRs, neutrinos, and GWs were used for astrophysical observations. From radio ( $\sim$ GHz) to  $\gamma$ -ray bands ( $< 1$  TeV), the telescopes and observatories, such as the Very-Large Array (VLA), Atacama Large Millimeter/submillimeter Array (ALMA), Hubble Space Telescope (HST), James Webb Space Telescope (JWST), Chandra X-ray Observatory, Swift Telescope, and the *Fermi* Space Telescope, can typically achieve decent angular resolution and flux sensitivities, which leads to the expanding samples of the sources and increasingly

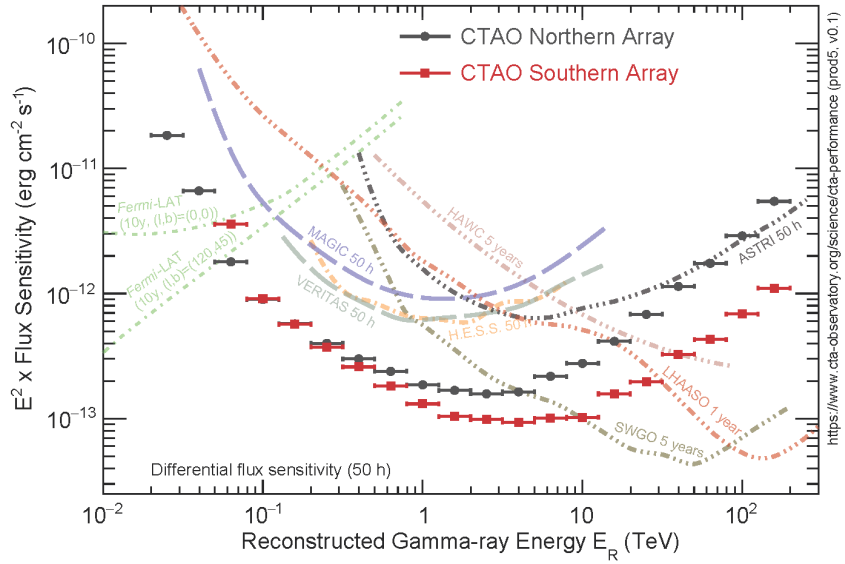


**Figure 1.1.** Differential sensitivities for CTA (50 hours), MAGIC (50 hours), VERITAS (50 hours), HESS (50 hours), HAWC (5 years), LHAASO (1 year), SWGO (5 years), and *Fermi* Large Area Telescope (*Fermi*-LAT), to obtain  $5\sigma$  detection of a point-like source.

precise models. In the higher energy range between 100 GeV and 100 TeV, the ground-based Imaging Air Cherenkov Telescopes (IACTs), e.g., Major Atmospheric Gamma Imaging Cherenkov Telescopes (MAGIC), High Energy Stereoscopic System (HESS), Very Energetic Radiation Imaging Telescope Array System (VERITAS), and the High-Altitude Water Cherenkov Observatory (HAWC) [9] observe the luminous sources in the very-high-energy (VHE)  $\gamma$ -ray bands by measuring particle and electromagnetic cascades in the atmosphere or water tanks induced by the interactions between VHE  $\gamma$ -rays and the medium. The detection of VHE  $\gamma$  rays of the two GRBs, GRB 190114C [10, 11] and GRB 180720B [12], broadens our view of relativistic jets and shocks, and demonstrates the great potential of the VHE  $\gamma$ -ray astrophysics. In the future, with the deployment and operation of the next-generation detectors such as the Cherenkov Telescope Array (CTA) [13] and the water Cherenkov detector array in the Large High Altitude Air Shower Observatory (LHAASO-WCDA) [14], we expect to see more distant  $\gamma$ -ray sources at TeV-PeV  $\gamma$ -ray energies due to their very wide energy ranges and excellent angular resolution and sensitivities (see Fig. 1.1).

From the multi-messenger point of view, contemporaneous multi-wavelength observations by different types of telescopes would be indispensable to distribute the alert to non-EM detectors and follow up the detections using other messengers. In practice, the

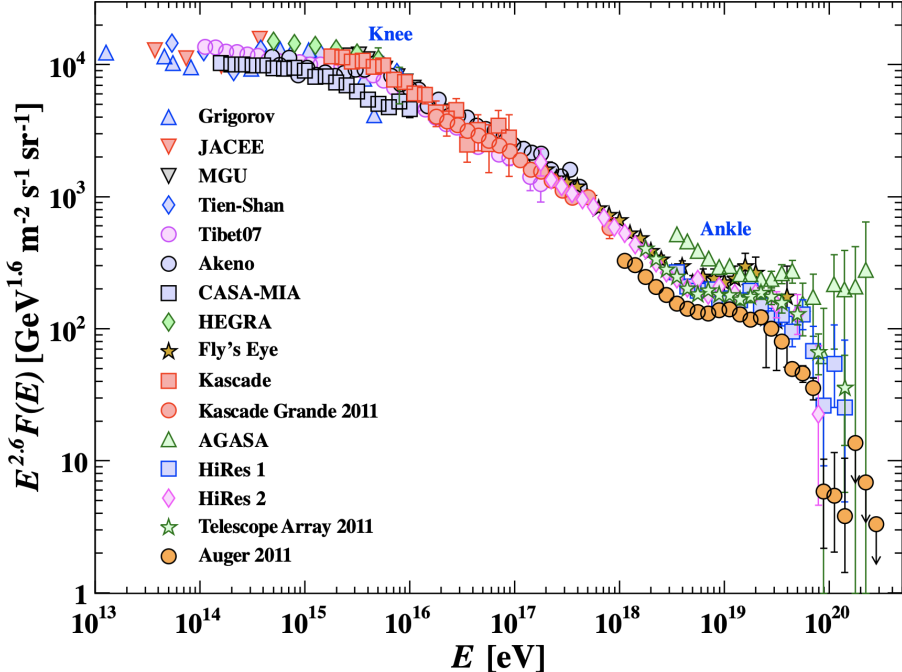


**Figure 1.2.** All particle CR energy spectrum (multiplied by  $E^{2.6}$ ) from air shower measurements [1]. See the text for a detailed description.

telescopes with a large field of view (FOV), e.g., the Square Kilometer Array (SKA), Large Spectroscopic Survey Telescope (LSST) [15], Swift, *Fermi*, and the Space Variable Object Monitor (SVOM) [16], can quickly localize the position of the target. After that, we can use the putative positional information from the initial follow-up imaging to guide the observation of narrower FOV telescopes. The Zwicky Transient Facility (ZTF) [17] will play an important role in generating real-time alerts for transients in optical bands and determining the significance of multi-messenger follow-ups.

### 1.1.2 Cosmic Rays (CRs)

In the early 20th century, Victor Hess first discovered the CRs in his balloon experiment by determining that the radiation intensity increases with altitude. Over the past few decades, the spectrum of CRs has been measured up to the EeV ( $10^{21}$  eV) range. However, its origin is presently unclear.

CRs are charged relativistic particles that can be described by a broken power-law over more than twelve orders of magnitude starting from  $\sim$  GeV (semi-relativistic) to multi-EeV (ultra-high-energy). Fig. 1.2 shows the differential energy spectrum of all-

composite CRs multiplied by  $E^{2.6}$  to display the changes in the spectral index. Below the knee ( $\sim 10^{15}$  eV), the observed spectrum  $E^{-2.6}$  is consistent with the superposition of the diffusion coefficient  $D(E) \propto E^\delta$  in the Milky Way, and the injected spectrum  $E^{-2}$  predicted by diffuse shock acceleration (also known as Fermi acceleration) [18]. It is generally believed that the galactic supernova remnants (SNR) dominate the CR injections in this energy range [19]. Between  $\sim 10^{15}$  eV and  $\sim 10^{18}$  eV (the “ankle”), the spectral index changes to  $-3.0$ , e.g.,  $F(E) \propto E^{-3.0}$ . Such a steepening might be caused by either a change of the diffusion regime or the cut-offs of the individual elements of the galactic component [1, 20, 21]. Above the ankle, the magnetic field in the Milky Way cannot trap these ultra-high-energy CRs (UHECRs), implying an extragalactic origin. The strong steepening at  $\sim 6 \times 10^{19}$  eV measured by the Pierre Auger cosmic ray observatory (Auger) [22] confirms the so-called GZK cut-off (named after Greisen, Zatsepin, and Kuz'min) [23, 24] caused by the interactions between UHECRs and cosmic microwave background photons. Considering the time delay ( $\Delta t \sim 10^4 - 10^5$  years) and the deflections ( $\Delta\theta \sim \text{several} \times 1^\circ$ ) while diffusing/propagating in the galactic and extragalactic magnetic fields, it would be very challenging to correlate the detected CRs to their sources.

The physical conditions of UHECR accelerators are stringently constrained: they should either have very strong magnetic fields or be very large. Given the typical turbulent magnetic field strength  $B$  and the size<sup>1</sup> of the accelerator  $R$ , we estimate the theoretical maximum energy of CRs [25]

$$E_{\text{cr,max}} \lesssim ZeBR, \quad (1.1)$$

where  $Z$  is the atomic number of accelerated particles. Specifying the CR energy, candidates that satisfy this requirement (for protons) are shown in Fig. 1.3 (the famous Hillas plot). The binary neutron stars, AGN jets, blazars, GRBs, and galaxy clusters can be promising UHECR sources. Since the high-energy astrophysical neutrinos are tightly associated with CRs, these UHECR accelerators are also regarded as important neutrino emitters.

### 1.1.3 High-Energy Astrophysical Neutrinos

Neutrinos were originally introduced by Pauli to particle physics to explain the continuous energy distribution in  $\beta$  decay experiment. They are natural particles that have a finite but very small rest mass, e.g.,  $m_\nu < 0.8$  eV/ $c^2$  at 90% confidence level from the latest

---

<sup>1</sup>For the relativistic jet with Lorentz factor  $\Gamma$ ,  $R = \Gamma \times \text{comoving size}$

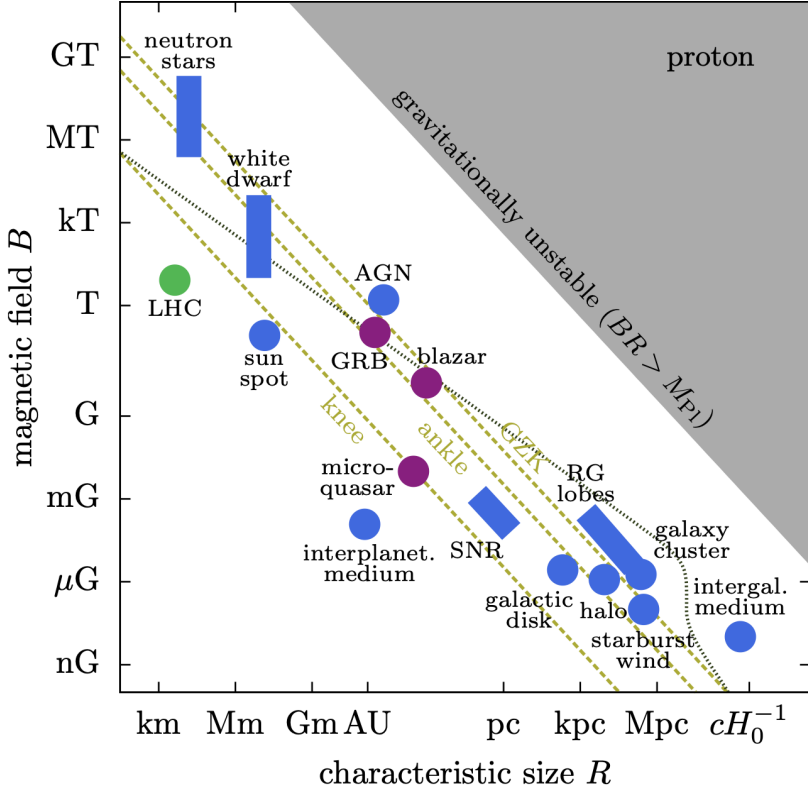


**Figure 1.3.** Source candidates that satisfy the Hillas criteria in the  $B$ - $R$  plane. The dashed lines correspond to the CR energies  $E_{\text{cr},\text{max}}=10^{14.5}$  eV (knee),  $10^{18.5}$  eV (ankle), and  $10^{19.6}$  eV (GZK).

direct neutrino-mass measurement [26]. Moreover, neutrinos only participate in weak interactions and can easily penetrate dense environments without significant attenuation. For PeV neutrinos, the interaction cross section with nucleons is  $\sigma_{\nu N} \sim 10^{-33} \text{ cm}^2$ , which is one hundred million times smaller than the Thomson cross section that measures the scattering between EM radiation and free charged particles. With this property, we can use astrophysical neutrinos as probes to study the innermost and densest regions of astronomical objects where photons cannot escape. On the other hand, we need to build very large detectors to capture these elusive particles.

Neutrino astrophysics has made substantial progress since the IceCube Neutrino Observatory in Antarctic [27, 28] (hereafter, IceCube) was completed. When a high-energy neutrino enters the detector, the neutrino will interact with the ice and produce secondary particles that travel through the detector at speeds close to  $c$ . In this process, Cherenkov light would be emitted and detected by the digital optical modules attached

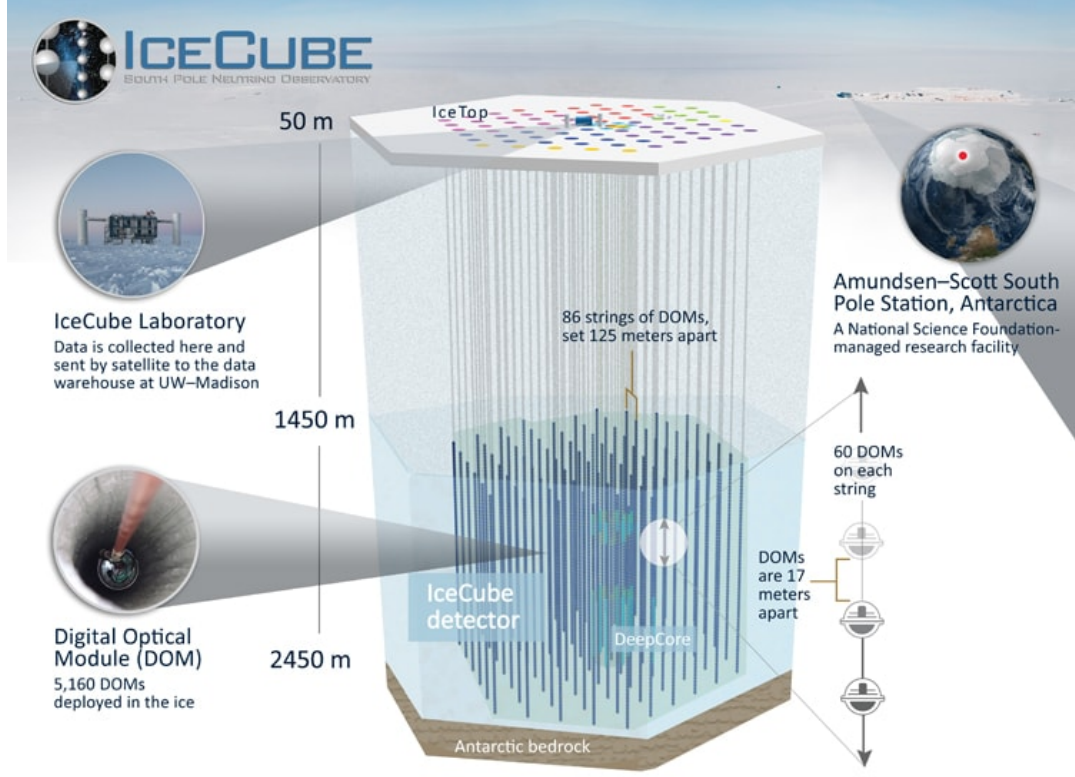


**Figure 1.4.** Schematic picture of the IceCube Observatory. IceCube is a cubic-kilometer detector located at the Antarctic. It consists of 5160 digital optical modules attached on 86 vertical strings. The detector measures the Cherenkov light from the secondary particles induced by the high-energy neutrinos.

to the vertical strings (see Fig. 1.4). We can then reconstruct the energy and arriving direction of the incoming neutrino using Cherenkov light patterns.

During the last half-decade, scores of high-energy (HE) astrophysical neutrinos with energies between  $\sim 10$  TeV and a few PeV have been detected by IceCube, and the number keeps growing [29–32]. The arrival directions of these neutrinos are compatible with an isotropic distribution even in the 10 – 100 TeV range, suggesting that a large part of these diffuse neutrinos come from extragalactic sources. Non-observation of diffuse Galactic  $\gamma$ -rays from the Galactic plane and other extended regions independently suggest that the Galactic contribution (e.g., by Fermi bubbles or local supernova remnants) is unlikely to be dominant [33–36]. However, despite extensive efforts, the physical nature of the sources of the diffuse neutrinos still remains in dispute. Possible candidates include gamma-ray bursts (GRBs) [37–43], low-power GRBs [44–50], radio-loud active galactic nuclei (AGNs) [51–59], radio-quiet/low-luminosity AGNs [60–63], and AGNs embedded

in galaxy clusters and groups<sup>2</sup>.

It is generally accepted that the bulk of astrophysical neutrinos are generated by charged pion ( $\pi^\pm$ ) decays, and that these pions are the secondaries from cosmic ray (CR) particles undergoing hadronuclear ( $p p$ ) or photohadronic ( $p \gamma$ ) interactions between the CRs and ambient target gas nuclei or photons. Meanwhile, these collisions also lead unavoidably to neutral pions ( $\pi^0$ ) as well, which subsequently decay into a pair of  $\gamma$ -rays. The relevant interactions can be written as

$$\begin{aligned}
p + p &\rightarrow p + \pi^\pm + \pi^0 + \dots \\
p + \gamma &\rightarrow n + \pi^\pm + \pi^0 + \dots \\
\pi^+ &\rightarrow \mu^+ + \nu_\mu \\
\mu^+ &\rightarrow e^+ + \nu_e + \bar{\nu}_\mu \\
\pi^- &\rightarrow \mu^- + \bar{\nu}_\mu \\
\mu^- &\rightarrow e^- + \bar{\nu}_e + \nu_\mu \\
\pi^0 &\rightarrow \gamma + \gamma \\
n &\rightarrow p + e^- + \bar{\nu}_e.
\end{aligned} \tag{1.2}$$

Hence, the diffuse neutrino flux is expected to have an intimate connection with the diffuse CR and  $\gamma$ -ray backgrounds, and multi-messenger analyses need to be applied to constrain the origin of these diffuse high-energy cosmic particle fluxes [64–66].

#### 1.1.4 Gravitational Waves (GWs)

GWs, the ripples of spacetime, are predicted by general relativity when the system generates a time-changing mass quadrupole moment. We expect the source to be massive and fast-accelerating to produce a detectable GW. The merging compact objects, including black holes and neutron stars, are the primary sources for the ground-based GW detectors that are sensitive in the high-frequency band, e.g., 10 Hz to  $10^4$  Hz. Experiments dedicated to the detection of GWs date back to the middle of the last century. In 2015, the first direct detection of GWs from a stellar-mass binary black hole (BH-BH) merger, GW150914 [67], by the Laser Interferometric Gravitational Wave Observatory (LIGO), not only tested the general relativity but also opened a new window to explore the Universe. Since then, the zoo of compact binary object (CBO) mergers, including BH-BH mergers, black hole - neutron star (BH-NS) mergers, and binary

---

<sup>2</sup>Groups of galaxies are smaller clusters, numbering from a few to dozens of galaxies.

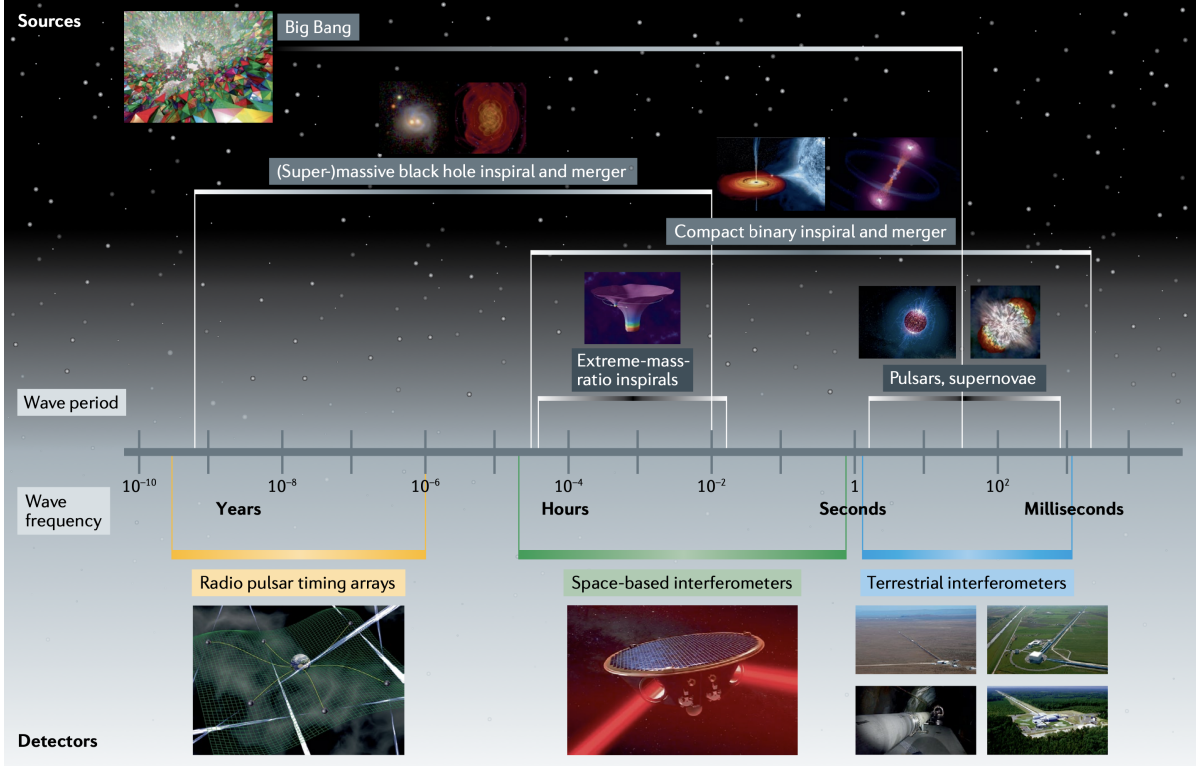


**Figure 1.5.** GW frequency bands of various source populations, ranging from  $10^{-9}$  Hz to  $10^4$  Hz [2]. GW telescope classes are shown below the frequency spectrum.

neutron star (NS-NS) mergers, keeps expanding in the observation runs of LIGO and Virgo interferometer (VIRGO). The LIGO-VIRGO observations of CBO mergers allow us to study the dynamics of compact binary systems in their last second before the coalescence and have profound implications to the physics of GRBs and kilonovae.

Fig. 1.5 depicts the GW frequency bands of various source populations, ranging from  $10^{-9}$  Hz to  $10^4$  Hz. The corresponding telescope categories are also listed. Ground-based interferometers such as LIGO, VIRGO, and future Japanese KAGRA will become the main force for observing the high-frequency GWs from  $\sim 10$  Hz to  $10^4$  Hz produced by CBO mergers and potentially the core-collapse supernovae. The upgrades to the current LIGO [68] and VIRGO, together with the involvement of future KAGRA and the LIGO-India interferometer, would significantly improve the ability of the LIGO-VIRGO-KAGRA network to detect and locate the GW events. The arm lengths of the current and future ground-based interferometers are typically multi-kilometers. The much longer arms are needed if we want to “sense” the low-frequency GWs. The next-generation space-based missions, such as the Laser Interferometer Space Antenna (LISA) [69], will play a leading role in detecting the low-frequency GW signals, e.g.,  $10^{-4}$  Hz - 1 Hz,

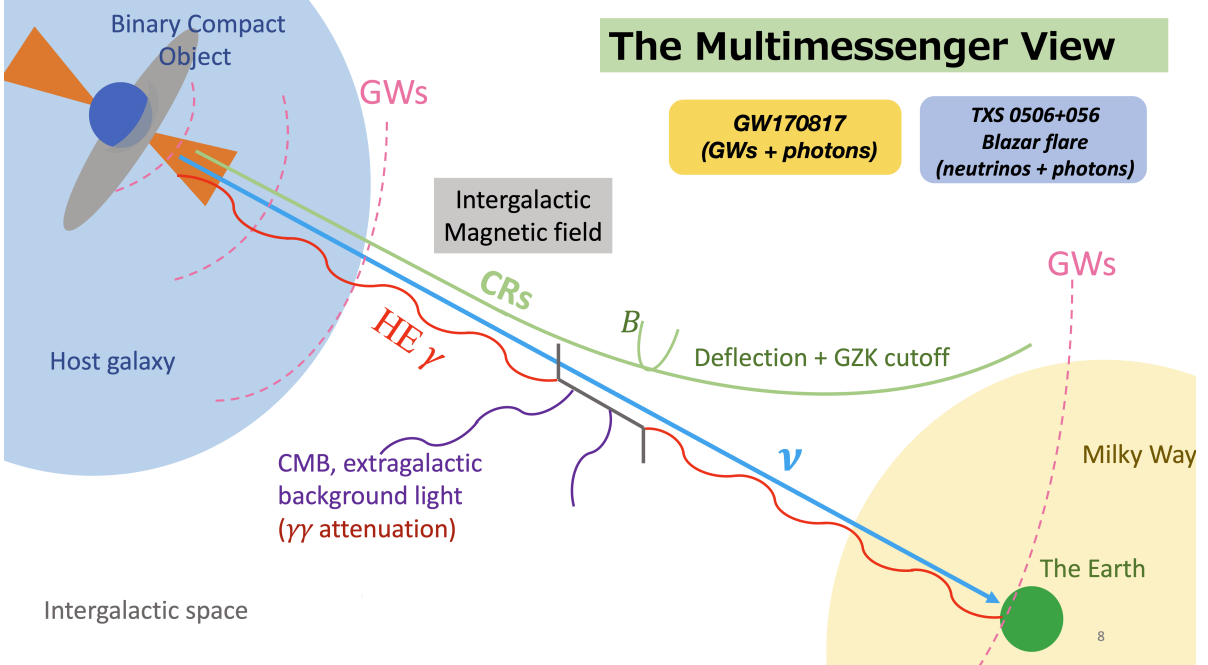


**Figure 1.6.** A schematic demonstration of the propagation of astrophysical messengers (high-energy  $\gamma$ -rays, neutrinos, GWs, and CRs) after leaving the source.

benefiting from the larger separation ( $\sim 2.5 \times 10^9$  m) between each satellite. The massive and supermassive black hole (SMBH) mergers in the mass range  $10^3 - 10^7 M_\odot$  are the dominant sources in this frequency band. Unlike the laser interferometer GW detectors mentioned before, the pulsar timing array works with the radio pulse from an array of millisecond pulsars that are  $\sim$  few  $\times$  0.1 kpc away from the Earth. Using PTA, we can explore the extremely low frequency ( $10^{-9}$  Hz –  $10^{-6}$  Hz) GWs from  $10^7 - 10^{10} M_\odot$  SMBH coalescences [70].

### 1.1.5 The Physical Picture of Multi-Messenger Astrophysics

The joint study of different messengers (EM photons, neutrinos, GWs, and perhaps CRs) can provide a holistic view of the physical processes and configurations of the sources. Fig. 1.6 schematically demonstrates how the messengers may propagate and what kind of interactions they may undergo before reaching the Earth. The high-energy  $\gamma$  rays can annihilate with other lower energy background photons, such as those from the extragalactic background light (EBL) and the cosmic microwave background (CMB). As a result, the  $\gamma$  rays from distant sources, e.g.,  $z \gtrsim 0.1$ , with energy  $E_\gamma \gtrsim 100$  GeV will be significantly attenuated. During the propagation, the UHECRs will be deflected by

galactic and extragalactic magnetic fields. The GZK cut-off also limits the maximum energy of the detected CRs. On the other hand, due to the weak scattering between neutrinos/GWs and matter, we can observe the VHE astrophysical neutrinos and GWs that point directly back to their sources.

## 1.2 Astrophysical Mergers in the Era of Multi-Messenger Astrophysics

In this dissertation, we focus on three promising sources, including galaxy/cluster mergers, SMBH mergers, and short GRBs formed by CBO mergers that are embedded in AGN disks, for the joint detection with EM photons, neutrinos, and GWs. In this section, we provide an overview of these astrophysical mergers and the motivation of our work.

### 1.2.1 Galaxy and Cluster Mergers

In the standard hierarchical galaxy formation scenario, galaxies form inside extended dark matter halos. When dark matter halos merge, the galaxies in these halos also merge, and the collision of the cold gas in the merging galaxies leads to shocks on a galactic scale in the galactic interstellar medium (ISM) gas. Later in the process of cosmological structure formation, at lower redshifts where galaxy groups and galaxy clusters have started forming, mergers among the dark matter halos containing these groups and clusters are also expected. These mergers are very energetic and result in shocks in the intergalactic medium (IGM) gas of the participating groups/clusters. One vivid example is the Bullet Cluster [71, 72]. Both these galactic and group/cluster shocks can accelerate CRs. The subsequent  $pp$  collisions between the shock-accelerated CRs and the thermal atomic nuclei in the gaseous environment are the major mechanism that generates HE neutrinos in these systems.

In chapter 2, we consider this scenario of both galactic scale shocks in the galactic ISM and group/cluster scale shocks in the intergalactic gas across redshifts. Whereas in a previous study [73] only galaxy mergers (mergers of two galaxies of approximately the same size) at  $z \sim 1$  were considered, here take into account the redshift evolution of the halo merger rate, and consider both galaxy and cluster mergers, including both major and minor mergers (the latter being those where the participating galaxies or clusters have mass ratios  $\zeta \neq 1$ ). We calculate the CR productions in the corresponding shocks at redshifts  $0 \leq z \leq 10$  and we find that high redshift ( $z \gtrsim 1 - 2$ ) halo mergers contribute a

significant part of the observed diffuse HE neutrinos and  $\gamma$ -rays without violating the non-blazar EGB constraint.

The  $pp$  interactions between accelerated CR and intergalactic medium can also generate high-energy non-thermal electrons and positrons (see Eq. 1.2). With the existence of galactic magnetic fields, these secondary particles can produce detectable radio and X-ray emissions via synchrotron and synchrotron self-Compton (SSC) processes. In chapter 3, we formulate a model which is capable of reproducing the radio and X-ray observations of specific systems using synchrotron and synchrotron self-Compton (SSC) or external inverse Compton (EIC) emissions from high-energy secondary electron-positron pairs produced by the CR interactions in such systems. Here the EIC is caused by scatterings with the cosmic microwave background (CMB), infrared/optical starlight (SL) and extragalactic background light (EBL). We show that our scenario can explain the observations of interacting galaxies, NGC 660 and NGC 3256. In addition, since the radiation spectrum of the merging galaxies is determined by the dynamics of the galaxy interactions and the resulting physical conditions, this enables us to provide constraints on the galactic magnetic field  $B$ , shock velocity  $v_s$ , galactic gas mass  $M_g$ , etc.

### 1.2.2 Supermassive Black Hole Mergers

Recent observations have provided increasing evidence that a large fraction of nearby galaxies harbors supermassive black holes (SMBHs). One influential scenario for the formation of these SMBHs is that they, like the galaxies, have grown their mass through hierarchical mergers (e.g., Ref. [74]). SMBH mergers are ubiquitous across the history of the Universe, especially at high redshifts where the minor galaxy mergers are more frequent. When galaxies merge, the SMBHs residing in each galaxy may sink to the center of the newly merged galaxy and subsequently form a SMBH binary [75, 76]. The SMBHs gradually approach each other as the gravitational radiation takes away the angular momentum, which eventually leads to their coalescence, accompanied by a GW burst. The GW burst from the final stage of coalescing can be detected by future missions such as LISA [77], providing through this channel valuable and prompt information about the merger rates, SMBH masses, and redshift. In addition, SMBH mergers are usually associated with mass accretion activities and relativistic jets, which may lead to detectable EM and neutrino emissions. For example, SMBH mergers may trigger AGN activities [78]. In this picture, the merger of SMBHs will become an important target for future multi-messenger astronomy (e.g., Ref. [79]).

Numerical simulations have demonstrated that SMBH mergers are typically accom-

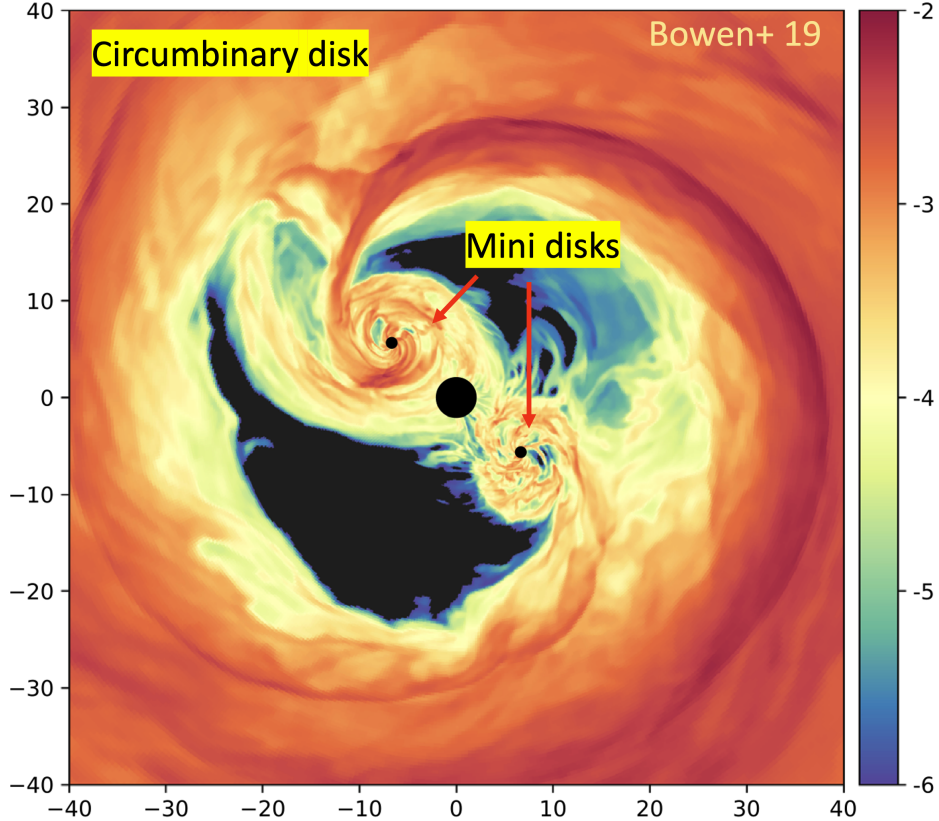


**Figure 1.7.** A snapshot of the density distribution of the circumbinary disk around the binary SMBH system and the mini-disks around each SMBH. The simulation was performed by Bowen et al. in 2019 [3].

panied by a circumbinary disk around the binary system (see Fig. 1.7 from [3]) and mini-disks surrounding each SMBH. The pre-merger circumnuclear material is thought to form from disk winds driven by the inspiralling binary SMBHs, in which a post-merger jet is launched, powered by the rotational energy of the remnant of the merger. In chapter 4, we present a concrete model for high-energy neutrino emission from four possible sites in the relativistic jet of SMBH mergers, namely, the collimation shock (CS), internal shock (IS), forward shock (FS), and reverse shock (RS). We show that month-to-year high-energy neutrino emission from the post-merger jet after the gravitational wave event is detectable by IceCube-Gen2 within approximately five to ten years of operation in optimistic cases where the cosmic-ray loading is sufficiently high and a mildly super-Eddington accretion is achieved.

In chapter 5, we study the EM emission produced in relativistic jets launched after the coalescence of SMBHs. The physical picture is that the disk winds originating from

the circumbinary disk and mini-disks around each SMBH form a pre-merger wind bubble, and jets powered by the Blandford-Znajek (BZ, [80]) mechanism are launched after the merger. The jets push ahead inside the pre-merger disk wind material, resulting in the formation of forward and reverse shocks. In the forward shock region, electrons are accelerated to high energies with a power-law distribution as observed in afterglows of gamma-ray bursts (GRBs) [81]. These particles then produce broadband non-thermal EM emissions through synchrotron and synchrotron self-Compton (SSC) processes.

### 1.2.3 Compact Binary Mergers

The (stellar-mass) compact binary mergers, including NS-NS mergers, NS-BH mergers, and BH-BH mergers, have attracted persistent interest in multi-messenger astrophysics due to the unique signatures in EM and GW observations. The evolution channel of a CBO depends on many factors. The two most prominent would be the mass distribution in the binary system and the environment. Fig. 1.8 depicts the evolution and the fate of a compact binary system. For instance, if the merger occurs in a gaseous environment, an accretion disk can be formed, and the super-Eddington accretion activity of the remnant would lead to a relativistic jet, which makes it a luminous  $\gamma$ -ray emitter. It is generally believed that short GRBs result from compact binary object (CBO) mergers [82–87], such as NS-NS mergers and potentially NS-BH mergers, whereas long GRBs are generated during the death of massive stars [88–93].

In 2017, the coincident detection of gravitational waves (GWs) and the corresponding electromagnetic counterpart from the binary neutron star merger GW170817, located in the host galaxy NGC 4933, marked a triumph of multi-messenger astronomy [94–96]. The spatial and temporal association between GW170817 and the  $\gamma$ -ray burst GRB 170817A also consolidates the theory that CBO mergers are the origin of short GRBs. Extensive efforts have shown that the broadband emission is consistent with a relativistic jet viewed from an off-axis angle [96–106]. Moreover, [107] investigated the upscattered cocoon emission as the source of the  $\gamma$ -ray counterpart. The long-lasting high-energy signatures of the central engine left after the coalescence was studied in [108].

Alternatively, unlike in the case of GW170817, one can expect a sub-population of short GRBs which occur in the accretion disks of AGNs. Studies of the CBO formation and evolution in AGN disks demonstrate that hierarchical mergers of embedded binary black hole systems are promising for reconstructing the parameters of LIGO/VIRGO detected mergers [109–112]. These mergers can harden the black hole mass distribution [113–116] as well. [117] pointed out that mergers involving neutron stars, such as GW190814 and

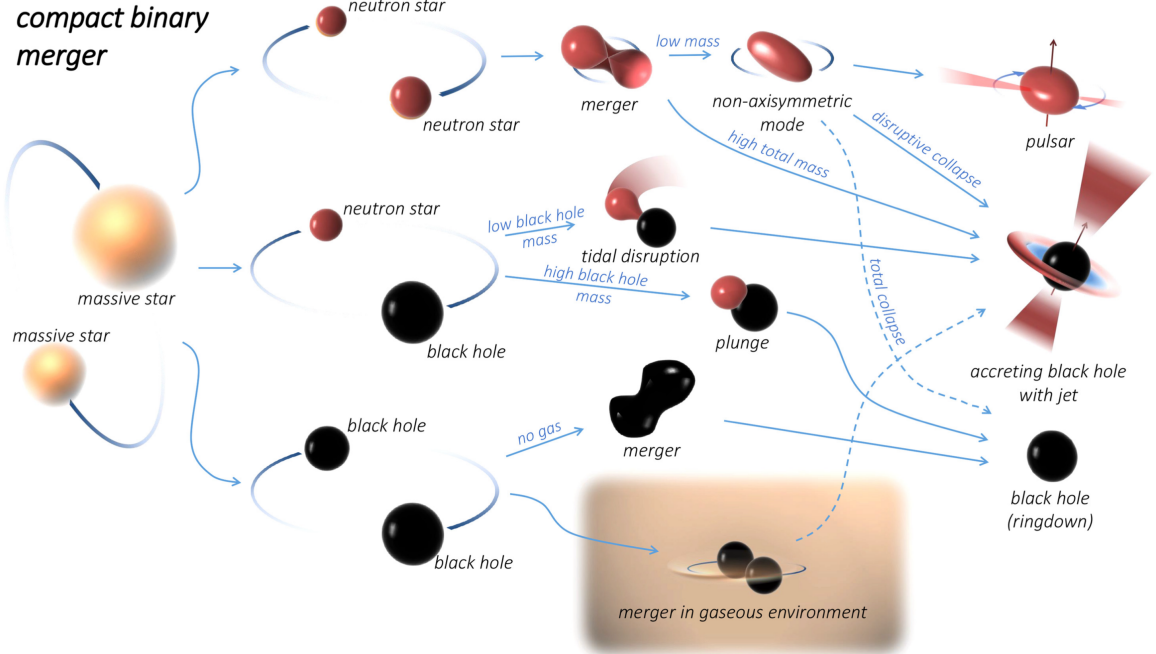


**Figure 1.8.** Evolution channels and fates of compact binary mergers including NS-NS mergers (upper channel), NS-BH merger (middle channel), and BH-BH mergers (bottom channel). Credit: Imre Bartos and Marek Kowalski [4].

GW190425, could also arise in AGN disks. Recent progress on the optical counterpart to GW190521 could support this [118], although the confirmation needs further observations [119]. [120] systematically studied the electromagnetic signatures of both long GRBs and short GRBs in AGN disks and discussed the conditions for shock breakout. [121] and [122] focused more on the neutrino production of embedded explosions. However, [123] showed that CBO environments are likely to be thin because of outflows that are common in super-Eddington accretion.

In chapter 6, we study  $\gamma$ -ray emission from short GRBs that are embedded in AGN disks. Inside the accretion disk, the embedded objects can migrate towards a migration trap due to angular momentum exchange via the torques originating from the disk density perturbations. At the migration trap, the gas torque changes sign, and an equilibrium is achieved as the outwardly migrating objects meet inwardly migrating objects. Numerical calculations show that compact binaries are typically formed near the migration trap at distances around  $R_d \sim 20 - 300R_S$  to the central supermassive black hole (SMBH, [124]), where  $R_S = 2GM_\star/c^2$  is the Schwarzschild radius. Employing one-dimensional N-body simulations, [115] obtained a more distant location for typical mergers at  $\sim 10^{-2} - 10^{-1}$  pc ( $\sim 10^3 - 10^4R_S$  for a SMBH with mass  $M_\star = 10^8M_\odot$ ). We concentrate on the embedded

GRBs with distances  $R_d \sim 10 - 10^3 R_S$ . We will show that AGN disks would not influence the  $\gamma$ -ray emission if the CBO mergers happen further outside in the disk. We also note that  $R_d = 10R_S$  is an extreme case where the population is stringently limited. The outflows from the binary systems with super-Eddington accretion rates are expected to form a low-density cavity-like structure before the merger occurs [123]. Within such a cavity, a successful GRB jet is likely to develop since the ambient gas density is not sufficiently high to stall the jet, in contrast to the choked-jet case discussed in [122]. Future multi-messenger analyses of AGN short GRBs can provide unprecedented insights for understanding the formation and evolution of CBOs inside the AGN disks as well as the origin of their high-energy emission.

## Constraints on Blazar Neutrinos

Blazars, including flat-spectrum radio quasars (FSRQs) and BL Lac objects, form a subclass of AGNs. They typically exhibit on-axis relativistic jets and dominant brightness in the  $\gamma$ -ray sky. Recently, the IceCube collaboration announced the spatial and temporal coincidence between a muon track neutrino event IceCube-170922A and a blazar TXS 0506+056 [125] at the significance  $\sim 3\sigma$ . Intuitively, if this association is physical, the intimate link between this IceCube neutrino event and the blazar may favor blazars as the main sources of the cumulative neutrino flux, but this is not the case [8].

The maximum likelihood stacking searches for cumulative neutrino flux from the second *Fermi*-LAT AGN catalog (2LAC) as well as the point-source searches using the IceCube muon track events and blazars in *Fermi*-LAT 3LAC have independently shown that *Fermi*-LAT-resolved blazars only contribute a small portion of the IceCube cumulative neutrino flux [126–128] and the hadronic models of blazar activity are strongly constrained [129], if the specific correlation  $L_\nu \propto L_{\text{ph}}$  is assumed as a prior. [130] evaluated the contribution of unresolved sources and showed that the blazar contribution to the cumulative neutrino flux is constrained unless one makes an *ad hoc* assumption that lower-luminosity blazars entrain a larger amount of CRs.

In addition to the stacking analysis, the absence of clustering in high-energy neutrino events, i.e., neutrino multiplets and auto-correlation, can also provide relevant constraints on various classes of proposed sources as the dominant origin of the cumulative neutrino flux [131–136]. The constraints are sensitive to the redshift evolution of the sources, which are especially powerful for weakly or non-evolving sources such as BL Lac objects [8, 131]. But the limits are weaker for rapidly evolving sources such as FSRQs, which could significantly alleviate the constraints, as remarked by [8]. [137] studied the constraints

on evolving blazar populations and confirmed that fast-evolving sources (e.g.,  $\xi_z = 5.0$ ) might indeed relax the neutrino multiplet limits.

In a separate effort, we study the stacking and multiplet constraints on the blazar contribution to the diffuse neutrino background in chapter 7. We consider the “joint” implications of these independent analyses for the global blazar population and extend the constraints to a common case where a generic relationship between neutrino and  $\gamma$ -ray luminosities, e.g.,  $L_\nu \propto (L_{\text{ph}})^{\gamma_{\text{lw}}}$ , is presumed, which is more general than what has been previously considered in such analyses. We treat  $\gamma_{\text{lw}}$  as a free parameter and attempt to reveal the  $\gamma_{\text{lw}}$ -dependence of the upper limits on all-blazar contributions. Our results show that these two limits are complementary and support the argument that blazars are disfavored as the dominant sources of the 100-TeV neutrino background. This work provides rather general constraints for future studies of blazar neutrinos.